Getting order in mesostructured thin films, from pore organization to crystalline walls, the case of 3-glycidoxypropyltrimethoxysilane

Davide Carboni,[a] Alessandra Pinna,[a] Heinz Amenitsch,[b] Maria F. Casula,[c] Danilo Loche,[c] Luca Malfatti[a] and Plinio Innocenzi[*a]

[a]Laboratorio di Scienza dei Materiali e Nanotecnologie, D.A.D.U., Università di Sassari, CR-INSTM, Palazzo Pou Salid, Piazza Duomo 6, 07041 Alghero (Sassari), Italy
[b]Institute of Inorganic Chemistry, Graz University of Technology, Stremayrgasse 9/IV, 8010 Graz, Austria
[c]Dipartimento di Scienze Chimiche e Geologiche, Università di Cagliari, 09042 Monserrato (CA), Italy.

ABSTRACT

A new type of mesostructured hybrid organic-inorganic film has been synthesised by evaporation-induced self-assembly using 3-glycidoxypropyltrimethoxysilane as precursor and a tri-block copolymer, Pluronic F127, as template. The chemistry has been tuned to form in the sol bridged polysilsesquioxanes that self-organize into ordered lamellar structures. Controlled aging in highly basic conditions, which has been monitored by Raman and infrared spectroscopy, has been used to obtain the layered ordered hybrid structures in the precursor sol. The pH of the sol has been adjusted to form the micelles that act as templates during solvent evaporation. Self-assembly of the system has been studied *in situ* by small and wide angle X-ray scattering using a synchrotron light source, which have confirmed both the formation of hybrid layered structures and the long-range organization of the mesophase in the hybrid films. The present approach allows ordering the hybrid film in two different length scales; at the end of film processing, hybrid crystals are retained into the pore walls and the micelles are arranged within the films with a long range order.

KEYWORDS: Hybrid organic-inorganic crystals, mesostructured films, sol-gel.

1. Introduction

Ordering mesoporous films through self-assembly is a kinetically driven process, which employs a supramolecular template for shaping and organising the mesostructure. In the evaporation induced self-assembly (EISA) processes, the evaporation of the solvent drives the formation and organization of micelles, while polycondensation of building blocks at the micelles interface gives rise to the mesostructure.[1] This process is now well known and several types of ordered mesostructures have been obtained.[2] Ordering the micelles and mastering their topology is, however, not the only type of issue at the nanoscale in mesostructured films.[3] Increasing the complexity of the material adding some new advanced properties, such as a higher durability and better mechanical properties, is a fundamental step for developing applications based on mesoporous films.[4] This target can be achieved through a careful design of the material properties, for instance the structure and composition of the pore walls, which form the material scaffold. Crystalline walls are easily obtained in films based on transition metal oxides, such as titania,[5] and even perovskite mesostructured films have been reported in literature.[6] Finally, also silica walls in mesostructured films have been crystallized using a seeding process with strontium or barium to assist quartz nucleation and growth.[7] In mesostructured crystalline oxide films the walls are generally formed by crystals of dimensions up to few nanometers while growth is achieved by a controlled thermal treatment. However, an increasing level of complexity arises if the walls are organic-inorganic; in this case they are formed through sol-gel reactions of organically modified alkoxides.[8] In general, organization in hybrid materials is observed only if bridged species are used to self-assemble into ordered layered structures.[9,10] At present, one of the few exceptions reported in literature is the case of 3-glycidoxypropyltrimethoxysilane (GPTMS), although this is not a bridged alkoxide; highly basic conditions are, in fact, capable of favouring the coupling of two GPTMS molecules, through reaction of the terminal epoxides, forming *p*-dioxane rings.[11] These newly formed molecules are substantially bridged species generated *in situ* that are eventually capable of self-organise themselves originating ordered layered structures.

Using these structures to create mesostructured materials through EISA processes is an even more difficult task because the kinetic of the evaporation does not allow an easy ordering of the layered hybrid material.[12] The first example of order into hybrid pore

walls of mesoporous materials has been given by Inagaki et al.[13], which have been able to produce layered structures using a 1,4-phenylene-bridged alkoxide. Following this first example, several other mesostructured materials with layered walls have been obtained, but only one clear example in films has been reported so far.[14] A biphenyl-bridged organosilica precursor, 4,4-bis(triethoxysilyl)biphenyl has been used for preparing mesoporous ordered films with molecular-scale periodicity in the pore walls *via* self-assembly. Interestingly, the synthesis and self-assembly have been carried out in mild acidic conditions, while a basic medium is generally used for synthesising powders. In basic solutions, self-assembly of the precursors into a lamellar organization is, in fact, directed by the hydrophobic-hydrophilic interactions between the fully hydrolysed bridged precursors $((HO)_3Si–R–Si(OH)_3)$.[15]

The formation of mesostructured ordered hybrid films, with ordered structures in the walls, is a process where, during evaporation, self-assembly has to be achieved in two different scales: at the molecular scale, with the formation of ordered lamellar structures, and at the meso-scale, with the organization of templating micelles. The chemistry and the kinetic of evaporation, which in films is much faster and therefore more critical, dictate the process. We have, therefore, tried to get order into a hybrid system without employing a preformed bridged alkoxide and concurrently studying *in situ* the self-assembly. 3-glycidoxypropyltrimethoxysilane has been used as the hybrid precursor and we have carefully designed the chemistry to have films with an ordered mesophase and a lamellar structure in the walls. To get order in both scales we have prepared a solution containing hybrid layered crystals, that we have allowed self-assembling around the templating micelles, obtaining an ordered mesophase within a crystalline hybrid films. Simultaneous small angle X-rays (SAXS) and wide angle X-rays scattering (WAXS) have allowed following *in situ* the organization at the two different length scales while the film morphology after thermal treatment has been observed by transmission electron microscopy (TEM).

2. Experimental

2.1 Chemicals

3-Glycidoxypropyltrimethoxysilane (GPTMS) (Sigma, >99%), ethanol (Sigma-Aldrich, > 99,8%), water (milli-Q), NaOH (Sigma-Aldrich, 35%) and HCl (Sigma-Aldrich, 37%), tri-block copolymer Pluronic F127 (PEO_{106}-PPO_{70}-PEO_{106}, Aldrich) were used as received without further purification. Silicon wafers (Si-Mat) (100) cut, *p*-type boron doped, 350 μm thick were used as substrates for film deposition. A cleaning solution MICRO-90® Aldrich was diluted to give a 10% v/v solution in water. The silicon wafers were cleansed with the 10% v/v cleaning solution, then washed thoroughly with water, acetone and finally with ethanol before drying them with compressed air.

2.2 Synthesis of the precursor sols.

The precursor sol was prepared by mixing 5 ml of GPTMS (5.350 g, 22.64 mmol, 1 eq.) with 2 ml of 2 M aqueous NaOH (0.16 g, 4 mmol, 0.18 eq.) in a glass vial. The solution was left to react for 30 minutes after which the vial was closed with a screw cap and left under stirring for 24 h. The sol was then aged for 8 days in a sealed vial.

2.3 Synthesis of hybrid organic-inorganic films

2.3.1 Deposition of hybrid films. 1 ml of ethanol was added to 1 ml of the aged sol (3.23 mmol of GPTMS, 1 eq.) and the pH of the resulting mixture was then adjusted to 7.5 by adding 0.350 ml of 2M aqueous HCl. The solution was left stirring and the films deposited with a withdrawal rate of 15 cm s^{-1} and a relative humidity of 25% at room temperature. The mesostructured films were deposited by following the same procedure but adding 0.47 mg of Pluronic F127 (0.35 mmol, 0.11 eq.) to the sol before changing the pH of the solution. The hybrid films were placed on a hot plate at 60°C soon after the deposition to stabilise the structure and for further 1 h at 150°C under Argon atmosphere.

2.3.2 Sol prepared for in situ SAXS-WAXS analysis. The sol was prepared with the same procedure described above but the deposition was performed with the dip-coater placed inside the SAXS experimental hutch.

2.4 Materials characterisation.

Attenuated Total Reflection (ATR) infrared analysis was performed with an interferometer Bruker infrared Vertex 70v equipped with a Platinum ATR attachment. The spectra were performed by casting a drop of sol onto the diamond of the ATR attachment and the data were acquired in the range 4000–400 cm^{-1} by averaging 256 scans with 4 cm^{-1} of resolution. The baseline was fitted by a concave rubber band correction with OPUS 7.0 software.

Fourier transform infrared (FTIR) analysis was performed with an interferometer Bruker infrared Vertex 70v. The spectra were recorded in transmission mode between 4000–400 cm^{-1} by averaging 256 scans with 4 cm^{-1} of resolution. The background was evaluated by measuring the signal of a clean silicon wafer substrate; the baseline was fitted by a concave rubber band correction with OPUS 7.0 software.

X-Ray Diffraction (XRD) patterns were recorded using a Bruker diffractometer D8 Discover working in grazing incidence geometry with a Cu k_α radiation source and equipped with a Goebel mirror and a scintillator. Diffraction patterns were recorded with a step size of 0.05° and iterations of 0.5 s in 2D mode; the acquisitions were repeated until a good signal-to-noise ratio was achieved.

A Bruker Senterra confocal microscope working with a laser excitation wavelength of 532 nm at 12.5 mW of nominal power was used for Raman spectroscopy analysis; the spectra were recorded by averaging 30 acquisitions of 2 s.

The organization of the mesopohase was studied by *in situ* 2D grazing incidence small-angle X-ray scattering (GI-SAXS). The experiments were performed at the Austrian SAXS beamline at Elettra using a synchrotron electron storage ring light source. The energy was set at 8 keV (λ = 1.54056 Å) and the incident angle of the beam at 0.5° ± 0.1° to obtain the highest contrast between the GISAXS pattern and the background; a CCD detector (Dectris 2D Pilatus3 1M) was used to acquire the scattering patterns and the experimental configuration was optimised in order to acquire the signal in the range spanning from 1.5 to 14°. The dip-coating was performed with a home-made equipment customized to fit the experimental hutch. The films were deposited at RH of 25 % and a GISAXS pattern was acquired every 2 seconds starting 10 seconds after the deposition.

The patterns were obtained by averaging 3 different acquisitions with 2 seconds of exposure time. A final static GISAXS pattern was acquired for 30 seconds, 5 minutes after the deposition.

Structure images were taken using a transmission electron microscope (TEM) (JEM-2000 FX JEOL) operating at 200 kV. The samples were prepared by scratching the films and depositing the fragments on a carbon-coated copper grid. Pore size was estimated from line profile analysis performed on representative TEM images with ImageJ programme.

A Wollam-α spectroscopic ellipsometer with fixed angle geometry was used to estimate the thickness of the dense hybrid films deposited on silicon substrates by fitting the experimental data with a model for absorbing films on Si substrates. The fit showed an average mean square error (MSE) smaller than 33.

The nanoindentation analysis was performed by using a CSM Table Top Nanoindentation Tester (TTX-NHT) equipped with a head suitable for loadings from 0.1 up to 500 mN and a load resolution of 0.04 μN. The instrument is mounted on an anti-vibration support. The Young's modulus of the hybrid films was estimated by averaging a number of measurements with normal force ranging from 0.4 to 0.8 mN.

3. Results and discussion

The present work aimed at obtaining crystalline mesostructured hybrid films using hybrid layered crystals as nano building blocks for the pores walls. These units have been let to form into the precursor sol and then have been incorporated within the pore walls to give an ordered mesophase. GPTMS has been selected as the chemical precursor because of its peculiar chemical properties; in highly basic conditions is, in fact, able to form bridged structures, *via* opening and coupling of two epoxy rings, which self-organize into lamellar structures (**Scheme 1**). The high pH, around 14, is a mandatory condition to get organization since both the silica condensation and the epoxide opening are strongly slowed down in these conditions. In fact, if the silica network would condense faster than the epoxide opening, the newly generated diols would not have time enough to form the bridged species, hampering therefore the self-organisation into layered structures. The choice of the Pluronic F127 as surfactant has

6

been dictated by its molecular nature; in fact its polyethylene oxide chains would have a close interaction with the ethylene oxide moieties present into the layered crystals. An increased interaction would promote the capability of forming an organised mesophase at the micelles interface. Highly basic conditions, however, are not fully compatible with the use of Pluronic F127 as micellar template since this surfactant has a good solubility in neutral and acidic pH, but very poor solubility in basic conditions. On the base of these premises, we have specifically designed an experimental protocol that allows the precursor to be used for generating bridged species. Afterwards, these will be used to form the hybrid scaffold during the formation of an ordered mesophase.

3.1 Growth of hybrid crystals in liquid phase.

Previous work from our group has highlighted the GPTMS structural changes as a function of the sol aging time, under different pH conditions.[16,17] Controlling the structural modifications,[18] which occur with time in highly basic conditions, allows tuning the formation of ordered hybrid structures to be employed for self-assembly at the mesoscale.

To follow the formation of hybrid crystals, the sol has been analysed as a function of the aging time by Raman spectroscopy. **Figure 1a** shows the Raman spectra of the sol up to 8 aging days in the 1330 - 1220 cm^{-1} range; the Raman bands have been normalised to the -CH$_2$ wagging band of the propyl chain, at 1296 cm^{-1}. In this range falls the epoxide -CH$_2$ rocking band, peaking around 1256 cm^{-1}, which allows following the reaction of the epoxides opening as a function of the aging time.[19] The band decreases in intensity with time (**Figure 1b**), showing that the reaction is a slow process, which can allow the formation and organization of bridged species, in accordance to the sol design. After 8 aging days around 75% of the epoxides are finally opened.

As we have previously underlined, the formation of the silica network should be slowed down enough to avoid that it hampers the formation of organic chains. For this reason, besides the opening of the epoxy group, another important reaction to be kept under control is the condensation of the silica species. **Figure 2** shows the changes in the ATR FTIR spectra in the region of the silica signals, 1175 - 925 cm^{-1}; the arrows show the direction of the change in the bands intensity as a function of the aging time. Three different overlapped bands are detected, one at 1090 cm^{-1}, assigned to Si-O-Si

symmetric stretching, a second one assigned to silica stretching in cyclic species at 1022 cm^{-1} and a third at 970 cm^{-1}. The latter one, which increases in intensity with aging, is attributed, most likely, to the -CH$_2$-OH twisting vibrations of the primary alcohol formed as a result of the epoxide opening.[20]

Although in general the sol-to-gel transition is realized through polycondensation of Si-OH groups, however the reaction rate could be significantly slowed down if very highly basic or acidic conditions are employed.[21] This strategy has been used before for self-assemble mesostructured materials using supramolecular templates,[1] but it can be used also for achieving self-organization in hybrid materials based on GPTMS. On the other hand, as we have demonstrated in previous works,[22] highly basic conditions favour a fast initial hydrolysis of the alkoxides while slowing down the polycondensation reaction. These conditions create a peculiar chemical environment which promotes the formation of silica cyclic species from GPTMS,[21,23] in accordance to previous findings and literature.[1,24] In particular, large strainless cage T_n species such as $[RSiO_{1.5}]_{n=8,10}$, or silica structures[25,26] (T_n denotes a cage structure with n SiO$_{3/2}$ groups) are expected to form.[21] The presence of open cages in the system is confirmed by the infrared analysis; the cyclic species form at the initial stage of sol-gel reaction and slowly condense with aging, as shown by the decrease in intensity of the 1022 cm^{-1} band. Similarly an increase in the silica stretching band (1090 cm^{-1}) at high aging time, indicates that the open cages tend to condense with the proceed of sol-gel reaction, giving rise to the silica random network. The silica structure during the aging time remains "*soft*" enough to allow opening the epoxy ring and forming bridged species, which self-organize into layered structure. The simultaneous polycondensation of the inorganic and organic network is, in fact, a competitive process which has to be carefully controlled;[27] a faster polycondensation rate of the inorganic network hinders the formation of the organic network and *vice versa*.

The signature of the organic reactions is given by the Raman band at 1456 cm^{-1}; **Figure 3** shows the spectra within the 1520 - 1425 cm^{-1} range, where two main bands are detected, the first one around 1485 cm^{-1}, assigned to CH$_2$ scissoring and CH rocking in epoxy rings,[19] the second at 1456 cm^{-1} to CH$_2$ scissoring in the propyl chain.[19] This last band increases in intensity with aging time while the epoxide gradually looses intensity becoming a shoulder of the propyl chain scissoring band at the end of the aging time.

This suggests that, with the gradual opening of the epoxy ring, new species are formed; in fact, the increase of the 1456 cm^{-1} band with aging can be explained with the rise of the *p*-dioxane species.[28] In our previous works, this band has been well correlated with the formation of layered hybrid structures.[29] The self-organization process starts with opening of the epoxides in highly basic conditions and subsequent formation of diols (-CH$_x$-OH) that react in pairs to form *p*-dioxanes, which can now behave like bridged species.[21] The condensation of silica species finally triggers the self-organization of the newly formed bridged molecules, which pile themselves to give layered crystals (**Scheme 1**).

3.2 Ordering mesoporous hybrid films with crystalline walls

Once obtained a hybrid sol containing layered structures, the next step was to bring the complexity to a further level, fabricating mesostructured films. The main problem, as we have previously observed, is the formation of micelles based on polyethylene oxide chains, in basic conditions. To overcome this issue, we have then changed the pH of the sol to 7.5 by adding hydrochloric acid, improving thus the solubility of the tri-block copolymer Pluronic F127. Moreover, to control the self-assembly process through the evaporation, we have diluted the hybrid sol by adding an equivalent amount of ethanol. The resulting hybrid films, deposited by dip-coating using this sol, have shown the typical signature of ordered hybrid structures in XRD spectra (**Figure 4**). In fact, as described in a previous work, the lamellar structure of the hybrid crystals is strictly correlated to the diffraction peak at 9°. This increases in relative intensity, as a function of the aging time of the sol,[22] when compared to the peak at 5°,[22,30] which is due to the intermolecular correlation of siloxane chains in an amorphous state.[31] The broad diffraction peak is generally indicated as the basal peak and is, in agreement with current literature, the typical signature of layered structures.[32]

To gain a better understanding of self-assembly in the hybrid films and to clarify if the micelles self-organise into ordered arrays, we have also performed a specific experiment. The hybrid sol, aged for 8 days and containing Pluronic F127, was dip-coated *in situ* onto a silicon wafer and analysed using a synchrotron light source. The experimental setup has been designed using a GISAXS-WAXS configuration to perform the measure in a 2-theta range spanning from 1.5 to 14°. The reason for such a

choice has been dictated by the need of having simultaneous information on the mesophase organisation (low angular range) and further evidences of the hybrid crystallinity (high angular range) given the higher definition attainable with the high brilliance source of the synchrotron light. X-ray scattering measurement under grazing incidence conditions, in fact, allows maximizing the scattering coming from the film and this experimental configuration has given the possibility of collecting consecutive SAXS acquisitions in a time scale of few seconds, enabling the real-time monitoring of the self-assembly process.

The evolution of the time-resolved GISAXS experiment has been followed every 12 seconds starting 10 seconds after the deposition. A selection of SAXS images describing the structural evolution of the mesophase organisation with time is shown in **Figure S1** (see ESI, **Figure S1**). For clarity, a synoptic overview is, instead, illustrated by **Figure 5**, where the images (**a-d**) describe the acquisitions performed after 10, 34, 46 and 134 seconds from film deposition.

Figure 5a gives a representation of the structural film organisation at time zero, which is 10 seconds after the deposition. At this stage the solvent just started evaporating and no spots indicating any order have been detected. In **Figure 5b**, 34 seconds after the deposition, a faint halo depicting an arc starts appearing, indicating a mesostructural organisation lacking of a defined order, which, instead, emerges 12 seconds after in **Figure 5c** (46 seconds after deposition) as soon as the solvent evaporation induced the self-assembly. **Figure 5c** shows, in fact, two defined and four faint spots indicating an ordered structure. The organisation is further confirmed after 88 seconds (**Figure 5d**), corresponding to 134 seconds after deposition, where the spots defining the ordered mesostructure are more visible. With the purpose of evidencing both the ordered mesostructure and the crystallinity of the hybrid material, 5 minutes after the film deposition, a GISAXS-WAXS measurement has been performed covering the 2θ angular range between 1.5 and 14° and acquiring the data for 30 seconds. The resulting image is reported in **Figure 6**, where the faint spots have been highlighted with white and yellow circles and the arc correlated to the crystallinity of the hybrid material in the walls is evidenced with a curve. On the basis on previous studies, the analysis of the SAXS pattern could indicates that the organisation of the mesostructure can be referred to as $R\bar{3}m$, i.e. a rhomboedral stack of spherical micelles; this arrangement is coherent

with a face-centered cubic array of micelles and is sometimes referred as $Fm\bar{3}m$.[33] Following this attribution we have indexed the spots highlighted by a white circle as (100) and (110). The yellow circles, instead, indicate the spots due to multiple diffraction within the films.[34]

The radial integration of the GISAXS-WAXS image has been performed by using silver behenate as a reference and the result is reported in **Figure 7.** Comparing this pattern with that in **Figure 4**, a shift to higher 2θ degrees, which corresponds to lower d spacings for the sample acquired with a conventional diffractometer (5.2 and 9.4°), is observed. In this case the d spacings are, in fact, 1.7 and 0.9 nm, respectively. This shift is not surprising, since it is due to the thermal treatment performed to stabilise the sample, whilst the pattern derived from the GISAXS-WAXS radial integration (4.9 and 8.6°) has been performed *in situ*, soon after the deposition of the coating, and it corresponds to 1.8 and 1.0 nm d-spacing, respectively. This result implies that the interlamellar spacing is reduced by 1 Å because of the thermal treatment. However, the most important difference between the two acquisitions is correlated to the shape of the peaks and their relative intensities. The pattern derived from the WAXS acquisition is, in fact, characterised by a peak at 9° narrower when compared to that one acquired with a conventional diffractometer. This is mainly due to the higher brilliance of the synchrotron light source that allows determining with clarity both the crystalline nature and the mesostructure order of the hybrid materials.

The organization at mesoscopic level has been further investigated by TEM analysis (**Figure 8a** and **S2**). The TEM characterization has revealed a highly organized mesostructure formed by large domains of cylindrical channels arranged in a 2D-hexagonal fashion. Line plot analysis applied on representative images has allowed estimating the average pore size as 4.3 ± 0.4 nm and the pore walls as 3.3 ± 0.3 nm (**Figure 8b** and **c**). These results are not in agreement with the space group attributed to the mesostructure by GISAXS characterization, however it should be considered that the TEM characterization requires the films to be thermally treated before measures (150°C under inert atmosphere). GISAXS, on the contrary, has been performed in situ during the self-assembly process. The change in the mesophase organization, therefore, is likely due to the thermal treatment, which is necessary to increase the contrast between pores and pore walls. This is particularly true for the specific chemical

11

composition of these hybrid matrixes; all the attempts to study the sample morphology by TEM on as-deposited films resulted in a severe damage of the specimens due to the electronic beam. A close examination of the TEM images allows also detecting a fine "texture" which is due to the self-organization of the bridged moieties into a crystalline lamellar structure (**Figure 8d**). The *d*-spacing of the lamellae derived from the TEM analysis is 1.2 ± 0.3 nm; this value is in agreement with that obtained from the Scherrer equation applied to the XRD pattern of the thermally treated sample (**Figure 7**). A drawing of the final material is shown in **Figure 9**; the film exhibits a long-range pore organization and ordered hybrid lamellar structures embedded in the pore walls.

The film performances have been studied both in terms of hydrolytically and mechanical stability. The films have been immersed either in water and acidic ethanol solution (0.5 ml of 2 M HCl in 10 ml of ethanol) for increasing times up to 24 h. After this period, the films have been observed through a microscope without noticing any relevant damage in their structure such as cracks or delamination.

The mechanical stability has been tested by nanoindentation on a mesostructured crystalline film with a thickness of 1851 ± 10 nm (as estimated by ellipsometry) in comparison with a reference sample prepared from a not-aged sol (i.e. an amorphous mesostructured sample) with a thickness of 1765 ± 50 nm. Interestingly, the analysis could be performed only onto the crystalline mesostructured sample, while the amorphous reference resulted to be too soft for these measurements, even at very small loading (0.2 mN). The analysis has allowed estimating the Young's modulus (E) of the mesostructured crystalline films as 0.302 ± 0.015 GPa. The value is in the same order of magnitude of the elastic modulus measured in silica mesoporous thin films[35] and much higher if compared with other mesoporous organosilica systems.[36] This measure marks a clear difference in the mechanical stability between an amorphous and crystalline mesostructured films made by the same hybrid precursor.

4. Conclusions

The present work has explored the possibility of synthesising crystalline periodic mesostructured organosilica starting entirely from a monosililated precursor, such as 3-glycidoxypropyltrimethoxysilane, which is capable of forming new bridged species *in*

situ. The resulting bridged polysilsesquioxane self-assemble and grows up into hybrid crystals forming lamellar structures by controlled aging of the highly basic precursor sol. The addition of surfactant Pluronic F127 as micellar template and pH modification enables the deposition of a self-organised crystalline mesostructured hybrid film, whose formation has been confirmed by *in situ* GI-SAXS-WAXS analysis. The test of mechanical properties has shown how the films processing can affect the final properties of the materials. In fact, despite the same chemical composition and mesoscopic organization, a hybrid mesoporous film can show a significant Young's modulus or a poor mechanical stability depending on the organization at the nanoscale. The possibility of controlling the evolution of the epoxide opening can therefore allow the synthesis of hybrid films that can be further functionalised after formation of an ordered matrix, giving rise to a versatile crystalline hybrid mesostructured platform.

References

[1] C. J. Brinker, Y. Lu, A. Sellinger, H. Fan, *Adv. Mater.*, 1999, **11**, 579.

[2] K. C.-W. Wu, X. Jiang, and Y. Yamauchi*, J. Mater. Chem.*, 2011, **21**, 8934; H.-Y. Lian, Y.-H. Liang, Y. Yamauchi, and K. C.-W. Wu, *J. Phys. Chem. C*, 2011, **115**, 6581; Y.-T. Liao, C.-W. Huang, C.-H. Liao, J. C. S. Wu, and K. C.-W. Wu, *Applied Energy*, 2012, **100**, 75; K. Ariga, Y. Yamauchi, G. Rydzek, Q. Ji, Y. Yonamine, K. C.-W. Wu, and J. P. Hill, *Chem. Lett.*, 2014, **43**, 36; A. Ivanova, D. Fattakhova-Rohlfing, B. E. Kayaalp, J. Rathouský, and T. Bein, *J. Am. Chem. Soc.*, 2014, **136**, 5930.

[3] P. Innocenzi, L. Malfatti, T. Kidchob, P. Falcaro, *Chem. Mater.*, 2009, **21**, 2555.

[4] P. Innocenzi and L. Malfatti, *Chem. Soc. Rev.,* 2013, **42**, 4198.

[5] G. J. A. A. Soler-Illia, P. C. Angelomé, M. C. Fuertes, D. Grosso, C. Boissiere, *Nanoscale,* 2012, **4**, 2549.

[6] D. Grosso, C. Boissiere, B. Smarsly, T. Brezesinski, N. Pinna, P. A. Albouy, H. Amenitsch, M. Antonietti, C. Sanchez, *Nat. Mater.*, 2004, **3**, 787.

[7] A. Carretero-Genevrier, M. Gich, L. Picas, J. Gazquez, G. L. Drisko, C. Boissière, D. Grosso, J. Rodriguez-Carvajal, C. Sanchez, *Science,* 2013, **340**, 827.

[8] G. Soler-Illia, P. Innocenzi, *Chem.–Eur. J.,* 2006**, 12**, 4478.

[9] A. Chemtob, L. Ni, C. Croutxè-Barghorn, B. Boury, *Chem. Eur. J.,* 2014, **20**, 1790.

[10] F. Lerouge, G. Cerveau, R. J. P. Corriu, *New J. Chem.*, 2006, **30**, 1364.

[11] B. Menaa, M. Takahashi, P. Innocenzi, T. Yoko, *Chem. Mater.,* 2007, **19**, 1946.

[12] N. Mizoshita, T. Tania, S. Inagaki, *Chem. Soc. Rev.,* 2011, **40**, 789.

[13] S. Inagaki, S. Guan, T. Ohsuna, O. Terasaki, *Nature,* 2002, **416**, 304.

[14] M. A. Wahab, C. He, *Langmuir*, 2009, **25**, 832.

[15] M. Cornelius, F. Hoffmann, M. Froba, *Chem. Mater.* 2005, **17**, 6674.

[16] D. Carboni, A. Pinna, L. Malfatti, P. Innocenzi, *New J. Chem.*, 2014, **38**, 1635.

[17] L. Gabrielli, L. Connell, L. Russo, J. Jiménez-Barbero, F. Nicotra, L. Cipolla, J. R.. Jones, *RSC Advances* 2014, **4**, 1841.

[18] L. Gabrielli, L. Russo, A. Poveda, J. R. Jones, F. Nicotra, J. Jiménez-Barbero, L. Cipolla, *Chem. Eur. J.* 2013, **19**, 7856.

[19] I. M. Sapic, L. Bistricic, V. Volovsek, V. Dananic, K. Furic, *Spectrochimica Acta Part A,* 2009, **72**, 833.

[20] *Infrared and Raman Characteristic Group Frequencies*, G. Socrates, 3rd ed., John Wiley & Sons Limited, Chichester, UK, 2001.

[21] P. Innocenzi, C. Figus, T. Kidchob, M. Valentini, B. Alonso, M. Takahashi, *Dalton Trans*. 2009, 9146.

[22] C. Figus, M. Takahashi, T. Kidchob, T. Yoko, M. Piccinini, M. Casula, P. Innocenzi, *J. Sol-Gel Sci. Technol.,* 2009, **52**, 408.

[23] L. Matejka, O. Dukh, J. Brus, W. J. Simonsick, B. Meissner, *J. Non-Cryst. Solids* 2000, **270**, 34; L. Matejka, O. Dukh, D. Hlavat, B. Meissner, J. Brus, *Macromolecules* 2001, **34**, 6904.

[24] B. Orel, R. Jese, A. Vilcnik, U. L. Stangar, *J. Sol-Gel Sci. Technol*. 2005, **34**, 251.

[25] H. Yoshino, K. Kamiya, H. Nasu, *J. Non-Cryst. Solids,* 1990, **126**, 68.

[26] M. Bartsch, P. Bornhauser, H. Burgy, G. Calzaferri, *Spectrochim. Acta, Part A,* 1991, **47**, 1627.

[27] P. Innocenzi, G. Brusatin, M. Guglielmi, R. Bertani, *Chem. Mater.,* 1999, **11**, 1672; P. Innocenzi, G. Brusatin, F. Babonneau, *Chem. Mater.,* 2000, **12**, 3726; B. Alonso, D. Massiot, F. Babonneau, G. Brusatin, G. Della Giustina, T. Kidchob, P. Innocenzi, *Chem. Mater.*, 2005, **17**, 3172.

[28] I. Kanesaka, S. Kamide, *J. Raman Spectroscopy,* 1996, **27**, 401.

[29] P. Innocenzi, C. Figus, M. Takahashi, M. Piccinini, L. Malfatti, *J. Phys. Chem. A,* 2011, **115**, 10438.

[30] M. Takahashi, C. Figus, T. Kidchob, S. Enzo, M. Casula, M. Valentini, P. Innocenzi, *Adv. Mater.,* 2009, **21**, 1732.

[31] H. B. Park, J. K. Kim, S. Y. Nam, Y. M. Lee, *J. Membr. Sci.,* 2003, **220**, 59; C. Joly, M. Smaihi, L. Porcar, R. D. Noble, *Chem. Mater.,* 1999, **11**, 2331.

[32] X. Hou, R. J. Kirkpatrick, L. J. Struble, P. J. M. Monteiro, *J. Am. Ceram. Soc*., 2005, **88**, 943.

[33] L. Malfatti, T. Kidchob, S. Costacurta, P. Falcaro, P. Schiavuta, H. Amenitsch, P. Innocenzi, *Chem. Mater.*, 2006, **18**, 4553.

[34] M. P. Tate, H. W. Hillhouse, *J. Phys. Chem. C*, 2007, **111**, 7645.

[35] H. Fan, C. Hartshorn, T. Buchheit, D. Tallant, R. Assink, R. Simpson, D. J. Kissel, D. J. Lacks, S. Torquato, C. J. Brinker, *Nat. Mater.* 2007, **6**, 418.

[36] F. K. de Theije, A. R. Balkenende, M. A. Verheijen, M. R. Baklanov, K. P. Mogilnikov, Y. Furukawa, *J. Phys. Chem. B*, 2003, **107**, 4280.

Figures

Figure 1. a) Raman spectra in the 1330-1220 cm^{-1} range as a function of sol aging time. The spectra have been normalized to the -CH$_2$- wagging band of the propyl chain, at 1256 cm^{-1} (*). The arrow shows the evolution of the band as a function of sol aging time. The GPTMS Raman spectrum is shown as reference in the top layer. b) Amount of epoxy opening (%) as a function of aging time calculated from the change in intensity of Raman rocking band at 1256 cm^{-1}.

Figure 2. ATR FTIR spectra in the 1175-935 cm^{-1} range as a function of sol aging up to 9 days. The arrows show the direction of absorption band intensity changes with aging.

Figure 3. Raman spectra in the 1510-1425 cm^{-1} range as a function of sol aging up to 8 days. The arrow shows the direction of intensity change with aging.

Figure 4. XRD diffraction pattern of a hybrid films with Pluronic F127, prepared from a sol aged for 8 days.

Figure 5. GI-SAXS images of a mesostructured crystalline GPTMS film deposited on Si wafer. The patterns were acquired after 10, 34, 46 and 134 seconds.

Figure 6. Static GI-SAXS image of a mesostructured crystalline GPTMS film deposited on Si wafer. The pattern was acquired for 30 seconds, about 5 minutes after the film deposition.

Figure 7. Diffraction pattern obtained by the radial integration of the SAXS-WAXS image in Figure **6.**

Figure 8. a) Representative TEM image of the mesostructured film; b) enlargement showing the 2D ordered mesostructure; c) plot profile of the line shown in panel b; d)

17

FFT-filtered enlargement of the same TEM image highlighting the crystalline lamellar structure.

Figure 9. Schematic representation of the hybrid film containing lamellar layered hybrid crystals within a long-range close-packed mesostructure.

<p align="center">**Scheme 1.**</p>

<p align="center">**TOC**</p>

<p align="center">A new type of hybrid organic-inorganic film showing long-range ordered mesostructure and crystalline pore walls has been successfully prepared</p>
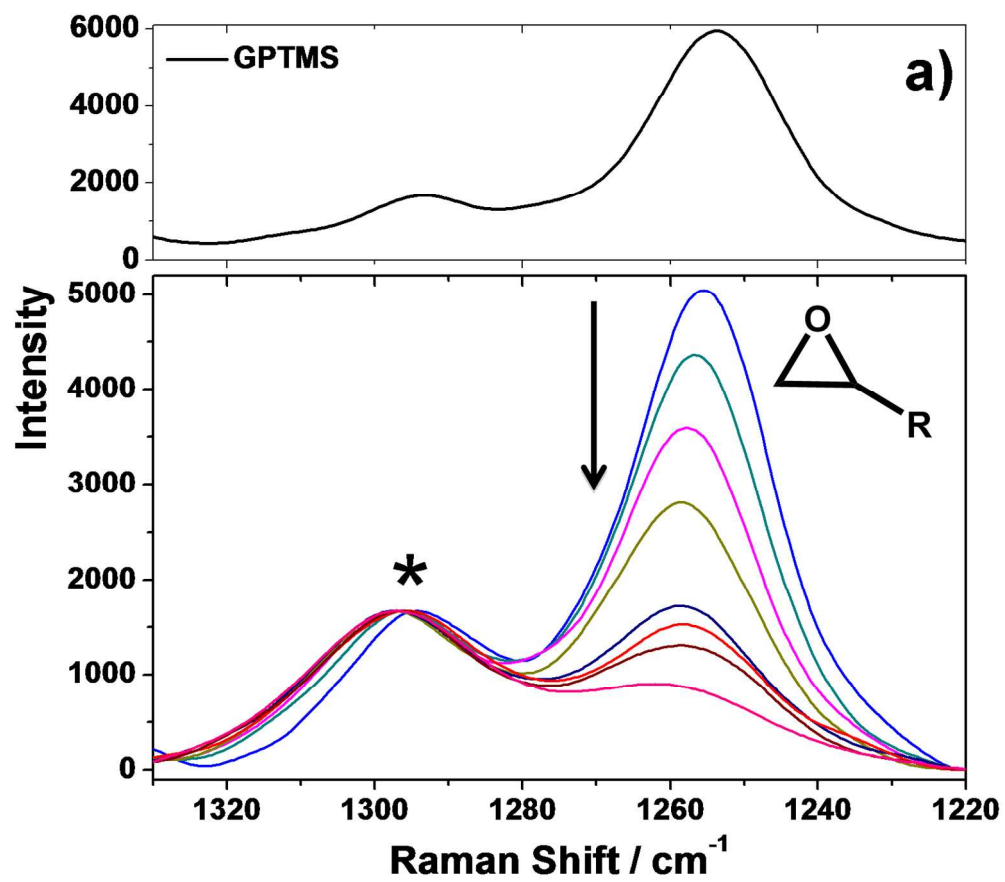
137x121mm (300 x 300 DPI)
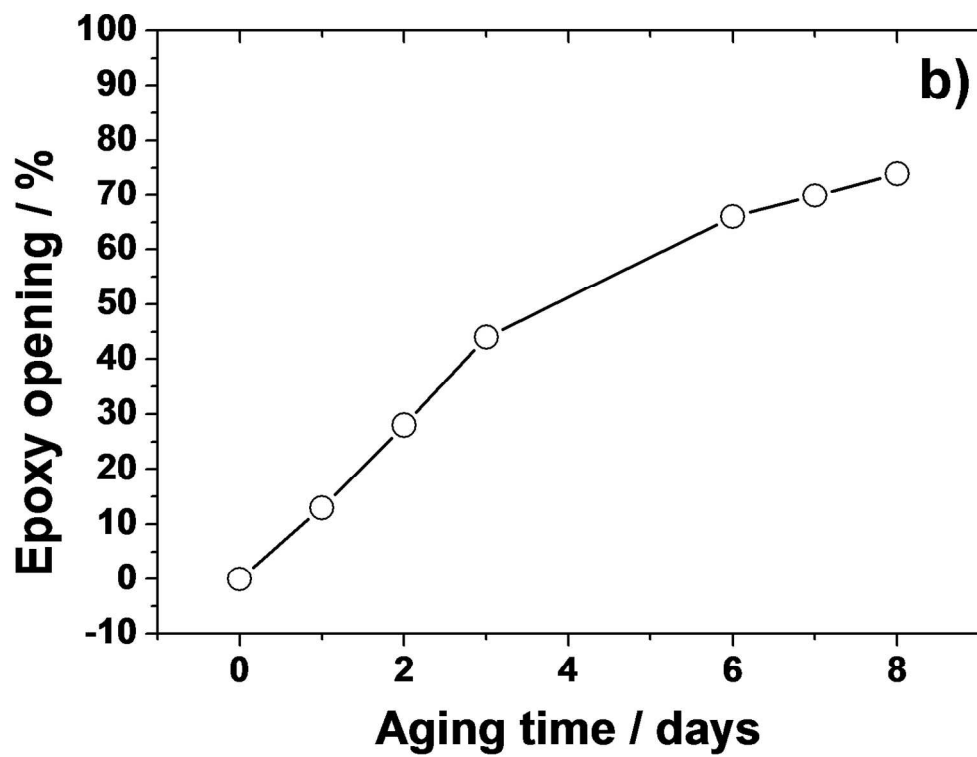
138x104mm (300 x 300 DPI)
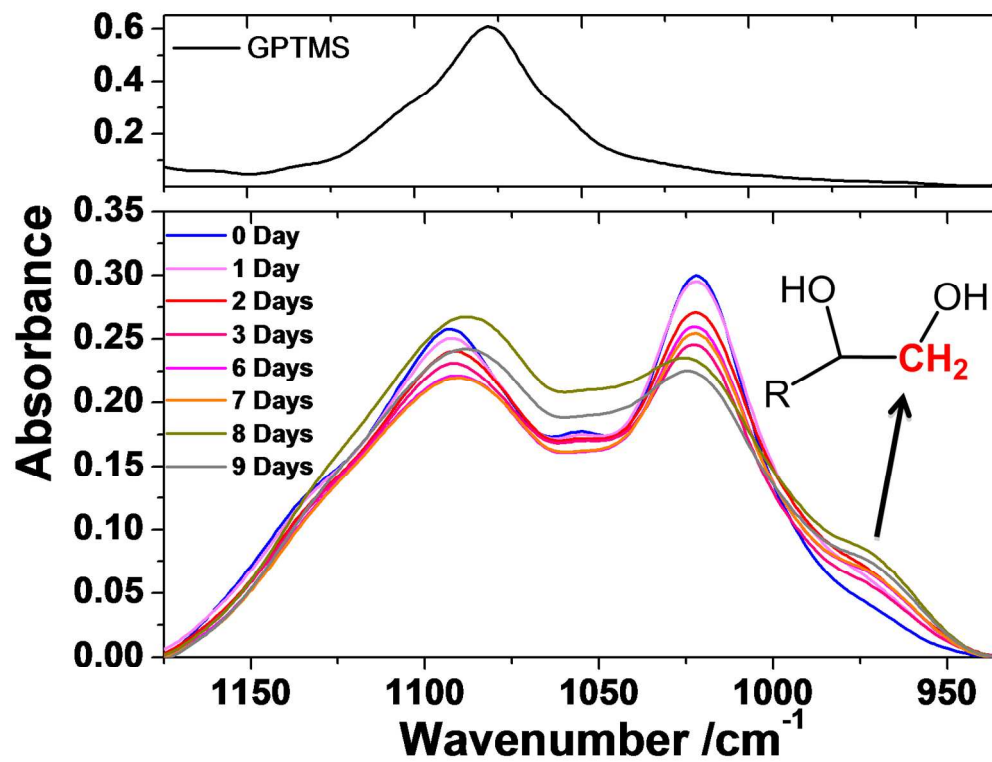
147x112mm (300 x 300 DPI)
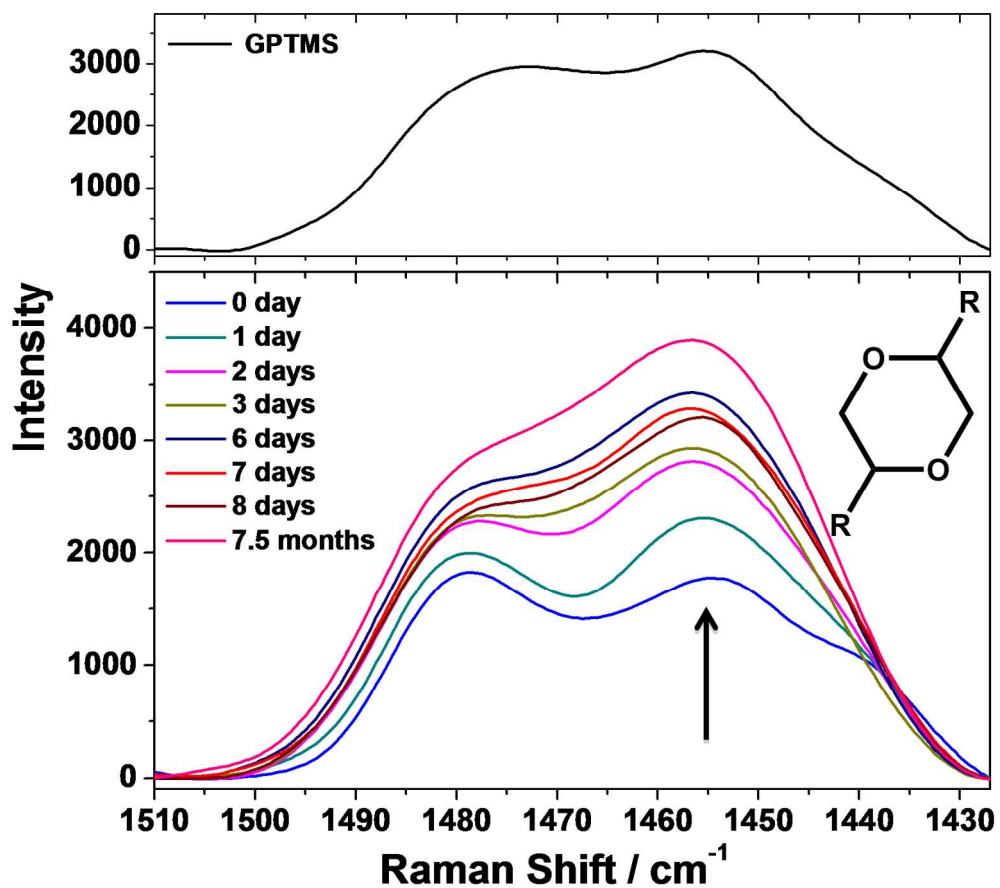
150x135mm (300 x 300 DPI)
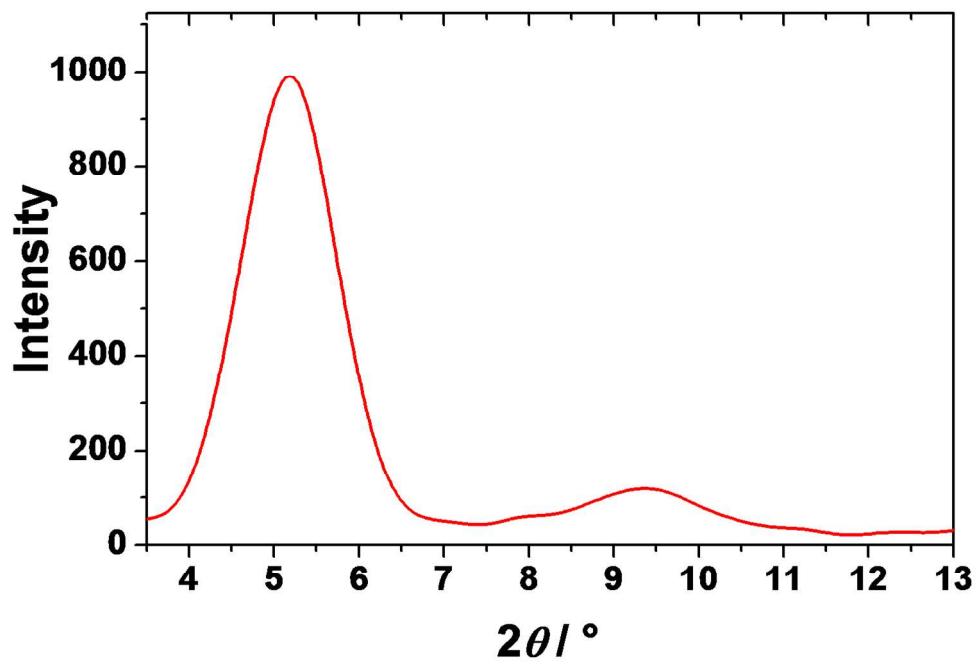
132x92mm (300 x 300 DPI)
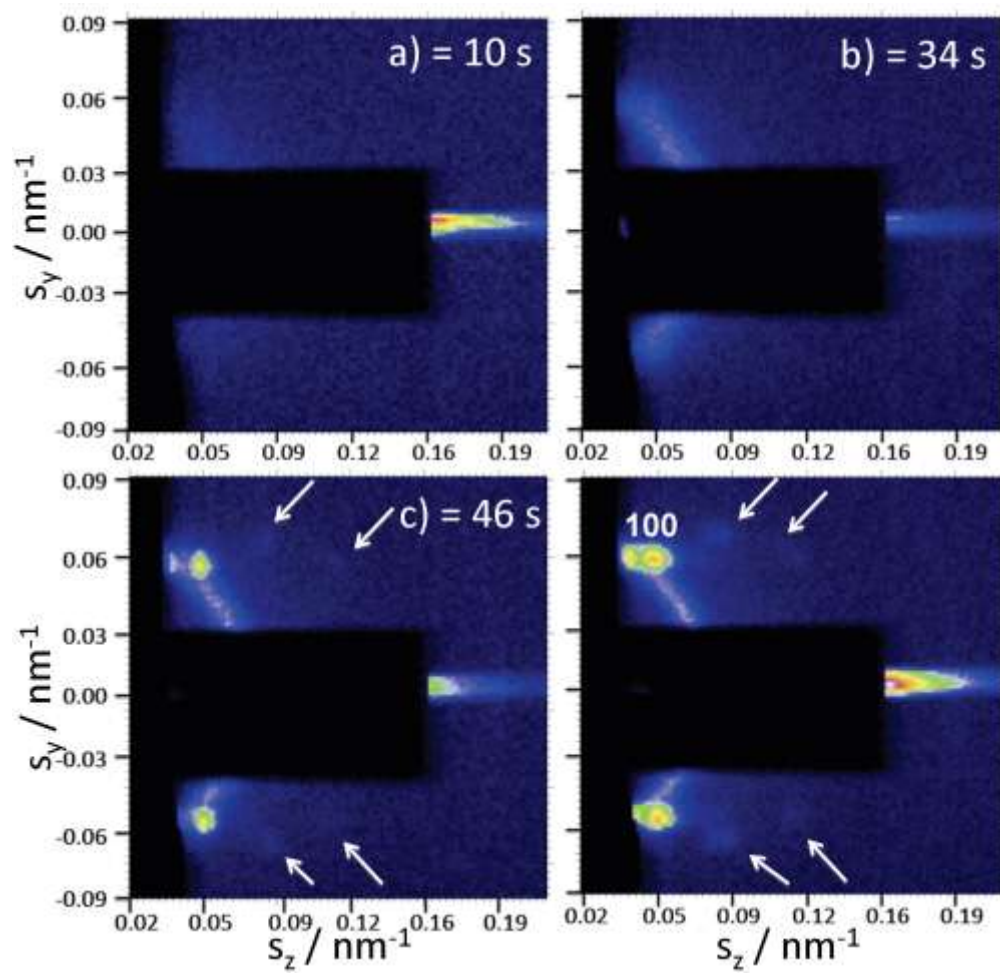
196x190mm (300 x 300 DPI)
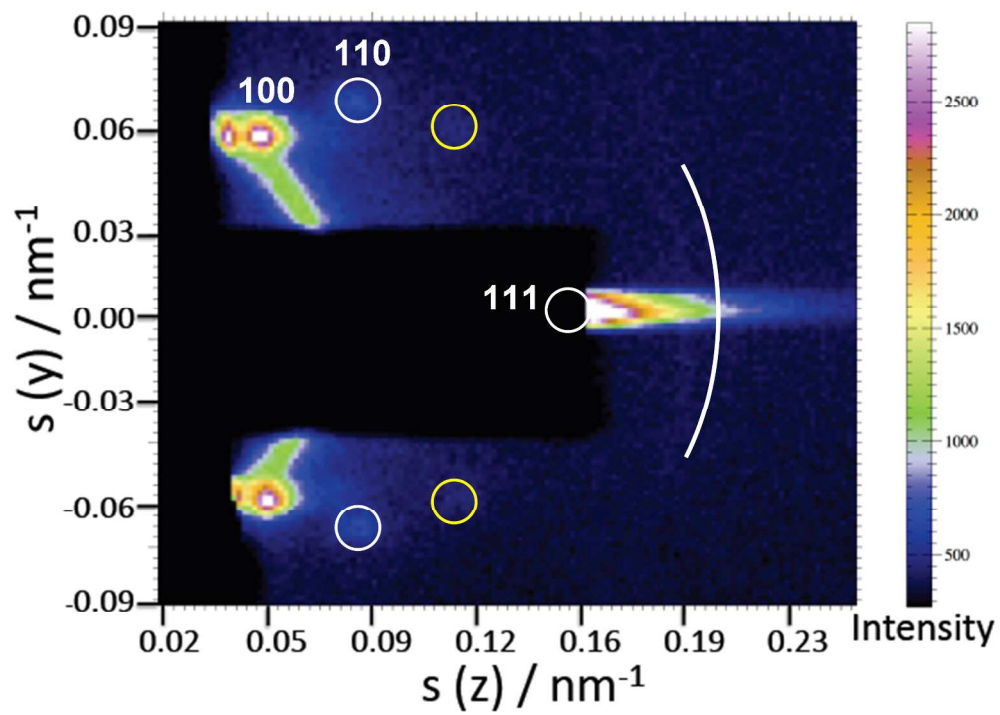
242x171mm (300 x 300 DPI)
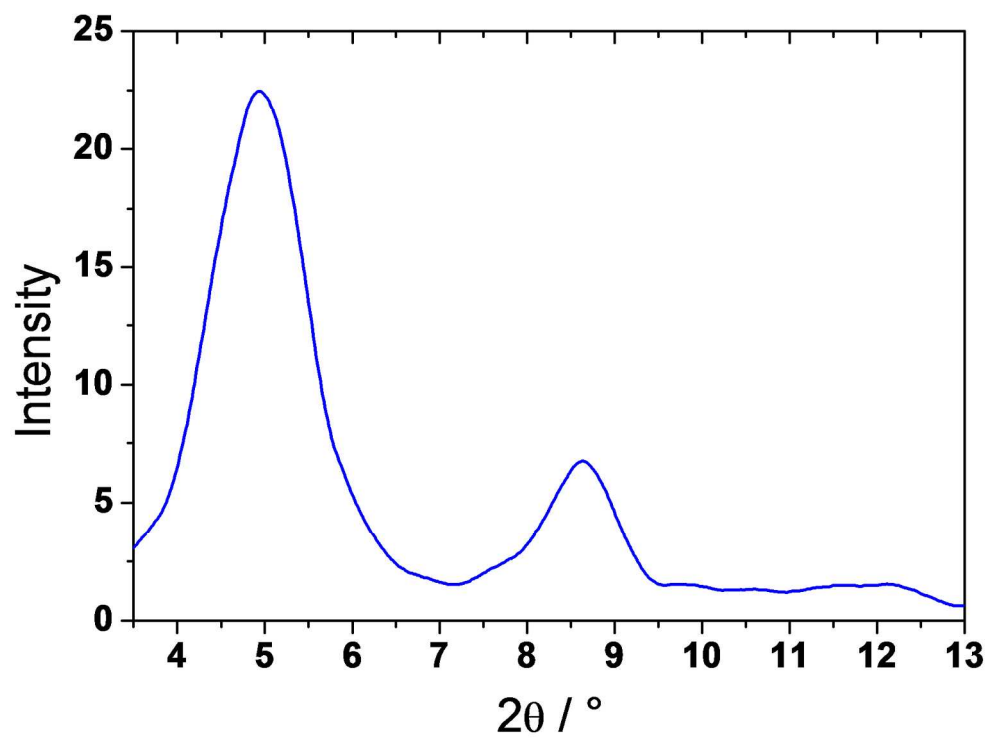
168x124mm (300 x 300 DPI)
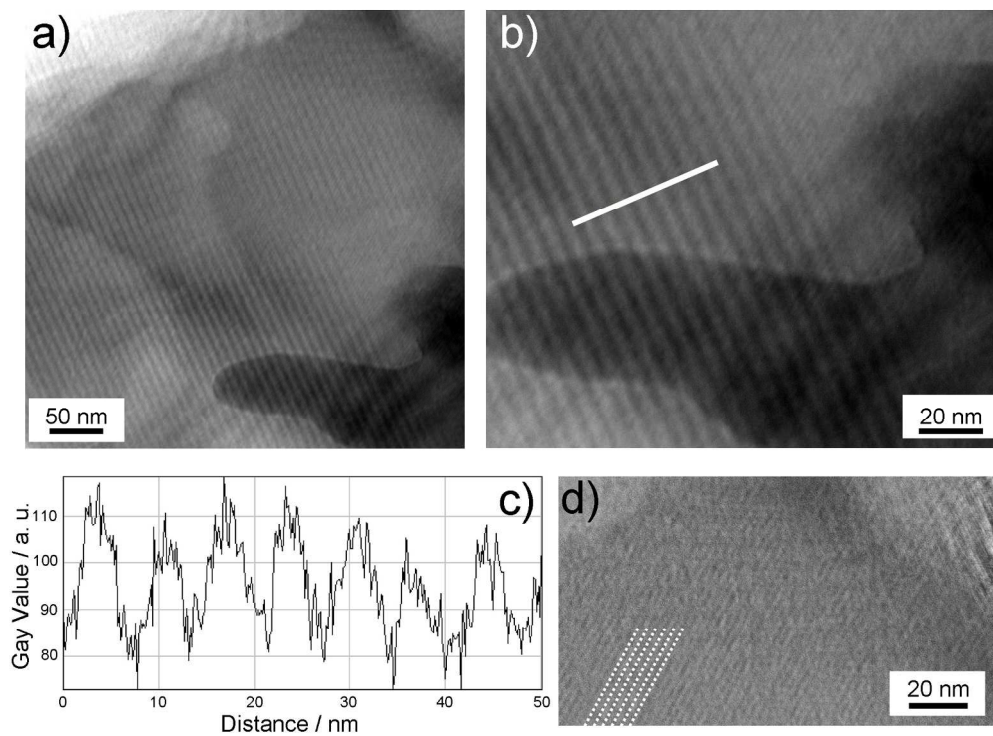
187x137mm (300 x 300 DPI)
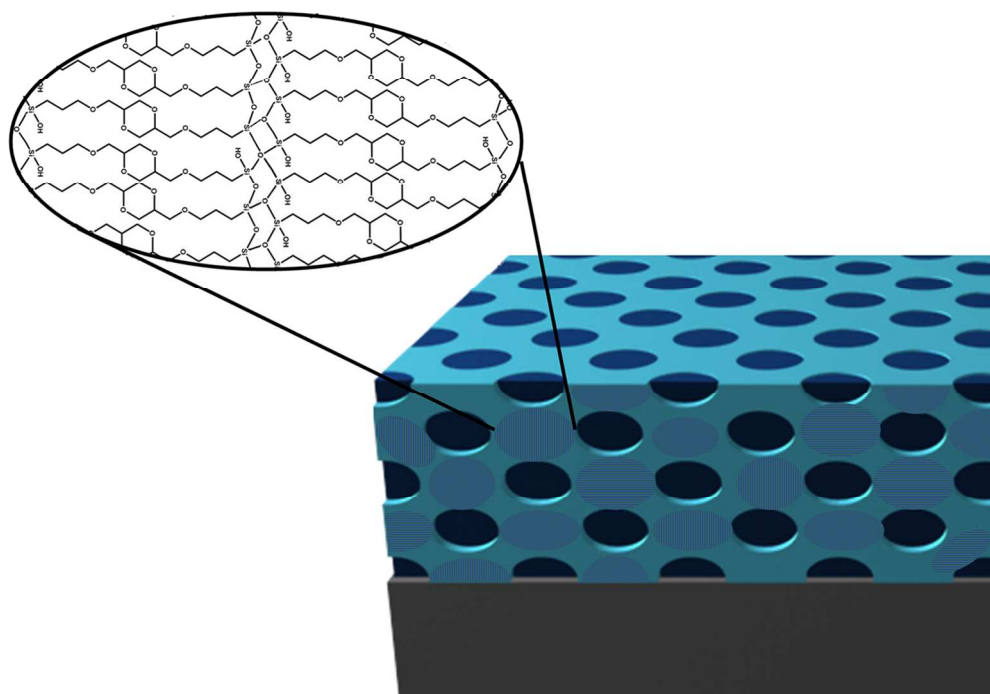
161x118mm (300 x 300 DPI)

223x130mm (300 x 300 DPI)